Weighted Median Filters Admitting Complex-Valued Weights and Their Optimization

Sebastian Hoyos, *Student Member, IEEE*, Yinbo Li, *Student Member, IEEE*, Jan Bacca, *Student Member, IEEE*, and Gonzalo R. Arce, *Fellow, IEEE*

***Abstract*—This paper introduces the concept of complex weighted median (WM) filtering admitting complex weighting. Unlike previous approaches in the literature that only allowed positive real-valued weights, the new WM structures exhibit improved performance as they exploit the richness of unrestricted complex weighting. To this end, the newly defined complex WM structures synthesize filtering operations, whereas the prior structures could only attain smoothing properties due to the inherent constraints imposed on the weights. In order to overcome the two-dimensional (2-D) search burden associated with the computation of the complex WM, two fast, robust, and very efficient approximations are introduced. Adaptive optimization algorithms for their design are developed leading to simple LMS-type weight updates. Several simulations are shown illustrating the performance of the new complex WM filter structures.**

***Index Terms*—Adaptive filters, complex filters, median filters, nonlinear filters, robust signal processing.**

I. Introduction

ALTHOUGH robust signal processing methods for real-valued data have been investigated extensively in the past decade, robust signal processing approaches for complex-valued signals have not received adequate attention. This is the case even for the well-known weighted medians (WMs), where complex weights are not admissible in the current structures. Even though the sorting and ordering of a set of complex-valued samples is not uniquely defined, as with the sorting of any multivariate sample set, the complex-valued median is well defined from a statistical estimation framework. The difficulties do not arise with the definition itself but with the computation of the complex-valued sample median that, in general, requires searching for the minimum of a cost function over the two-dimensional (2-D) complex field—a prohibitively expensive computational task. In addition, if weighting of the complex samples is desirable, the existing definitions of the complex-valued median are severely limited in that only positive weights are allowed. This, in essence, defines smoother structures that are inadequate in most engineering applications. A general complex-valued WM filter framework is of interest where the weights can take on complex values.

Several approaches to overcome the computation complexity of complex-valued medians have been proposed [1]–[3]. To date, however, none of the proposed structures allows for complex-valued weights. This paper establishes the definition of complex weighting in WM filters. Based on the concept of phase-coupling and real-imaginary coupling, we introduce complex-valued median filtering structures. Phase coupling emerges as a generalization of Arce's sign coupling concept used in real-valued WM filters [4]. The concept of real-imaginary coupling introduces a different approach of handling complex-valued weights in WM filters. In order to introduce the concept of phase coupling and real-imaginary coupling, it is useful to formulate the complex-valued WM filtering problem from its statistical roots.

The complex sample mean and sample median are two well known maximum likelihood (ML) estimators of location derived from sets of independent and identically distributed (i.i.d.) samples obeying the complex Gaussian and complex Laplacian distributions, respectively. Thus, if $X_i \in \mathcal{C}, i = 1, \ldots, N$ are i.i.d. complex Gaussian distributed samples with variance σ^2 [5] and constant but unknown complex mean β, the ML estimate of location is the value $\bar{\beta}$ that maximizes the likelihood function

$$\bar{\beta} = \arg\sup_{\beta} \left\{ \left(\frac{1}{\pi\sigma^2} \right)^N \exp\left(-\sum_{i=1}^{N} |X_i - \beta|^2/\sigma^2 \right) \right\}. \quad (1)$$

This is equivalent to minimizing the sum of squares as

$$\bar{\beta} = \arg\inf_{\beta} \sum_{i=1}^{N} |X_i - \beta|^2 = \text{MEAN}(X_1, X_2, \ldots, X_N). \quad (2)$$

Letting each sample X_i be represented by its real and imaginary components $X_i = X_{R_i} + jX_{I_i}$,[1] the minimization in (2) can be carried out marginally without losing optimality by minimizing real and imaginary parts independently as $\bar{\beta} = \bar{\beta}_R + j\bar{\beta}_I$, where

$$\begin{aligned} \bar{\beta}_R &= \arg\inf_{\beta_R} \sum_{i=1}^{N} (X_{R_i} - \beta_R)^2 \\ &= \text{MEAN}\,(X_{R_1}, \ldots, X_{R_N}) \end{aligned} \quad (3)$$

$$\begin{aligned} \bar{\beta}_I &= \arg\inf_{\beta_I} \sum_{i=1}^{N} (X_{I_i} - \beta_I)^2 \\ &= \text{MEAN}\,(X_{I_1}, \ldots, X_{I_N}). \end{aligned} \quad (4)$$

[1]The subindices R and I represent real and imaginary parts and will be used extensively throughout the paper.

Manuscript received October 8, 2002; revised October 24, 2003. The associate editor coordinating the review of this paper and approving it for publication was Prof. Ioan Tabus.

S. Hoyos was with the Department of Electrical and Computer Engineering, University of Delaware, Newark, DE 19716 USA. He is now with the Department of Electrical Engineering and Computer Sciences, University of California, Berkeley, CA 94720 USA (e-mail: mail@sebastianhoyos.com).

Y. Li, J. Bacca, and G. R. Arce are with the Department of Electrical and Computer Engineering, University of Delaware, Newark, DE 19716 USA (e-mail: yli@ee.udel.edu; baccarod@ee.udel.edu; arce@eecis.udel.edu).

Digital Object Identifier 10.1109/TSP.2004.834342

When the set of i.i.d complex samples obeys the Laplacian distribution, it can be shown that the ML estimate of location is the complex-valued estimate $\hat{\beta}$ that minimizes the sum of absolute deviations

$$\hat{\beta} = \arg\inf_{\beta} \sum_{i=1}^{N} |X_i - \beta|. \tag{5}$$

Unlike (2), the minimization in (5) cannot be computed marginally and, in general, it does not have a closed-form solution, requiring a 2-D search over the complex space for the parameter $\hat{\beta}$. The suboptimal approach introduced by Astola, referred to as the vector median [6], consists of assuming that the $\hat{\beta}$ that satisfies (5) is one of the input samples X_i. Thus, Astola's vector median outputs the input vector that minimizes the sum of Euclidean distances between the candidate vector and all the other vectors. Astola also suggested the marginal complex median, which is a fast but suboptimal approximation, by considering the real and imaginary parts independent of each other, allowing the breakup of the complex-valued optimization into two real-valued optimizations, leading to $\hat{\beta} \approx \tilde{\beta} = \tilde{\beta}_R + j\tilde{\beta}_I$, where $\tilde{\beta}_R = \text{MEDIAN}(X_{R_1}, X_{R_2}, \ldots, X_{R_N})$ and $\tilde{\beta}_I = \text{MEDIAN}(X_{I_1}, X_{I_2}, \ldots, X_{I_N})$.

When the samples are independent but not identically distributed, the ML estimate of location can be generalized. In particular, letting $X_1, X_2, \ldots, X_N$ be independent complex Gaussian variables with the same location parameter $\bar{\beta}$ but distinct variances $\sigma_1^2, \ldots, \sigma_N^2$, the location estimate becomes

$$\hat{\beta} = \arg\inf_{\beta} \sum_{i=1}^{N} W_i |X_i - \beta|^2 = \frac{\sum_{i=1}^{N} W_i \cdot X_i}{\sum_{i=1}^{N} W_i} \tag{6}$$

with $W_i = 1/\sigma_i^2$, which is a positive real-valued number. Likewise, under the Laplacian model, the ML estimate of location minimizes the sum of weighted absolute deviations

$$\hat{\beta} = \arg\inf_{\beta} \sum_{i=1}^{N} W_i |X_i - \beta|. \tag{7}$$

Once again, there is no closed-form solution to (7) in the complex-plane, and a 2-D search must be used. Astola's approximations used for the identically distributed case can be used to solve (7), but in this case, the effect of the weights W_i must be taken into account. These approaches, however, lead to constrained structures where neither negative or complex weights are admitted. To overcome these limitations, we introduce the concept of *phase coupling*, consisting of decoupling the phase of the complex-valued weight and merging it to the associated complex-valued input sample. This approach is an extension of the general WM (GWM) filter [4], where the negative sign of the weight is uncoupled from its magnitude and is merged with the input sample to create a set of signed-input samples that constitute the output candidates. The phase coupling concept is used to define the *phase-coupled* complex WM filter, which, unlike the GWM, does not have a closed-form solution, thus requiring searching in the complex plane. To avoid the high computational cost of the searching algorithm, a suboptimal implementation called *marginal phase-coupled* complex WM is presented.

A second approach to the weighting concept in the complex-domain is also introduced. This weighting technique exploits the correlation between the real and imaginary parts of the complex input samples. This second filter is called the *real-imaginary coupled* complex WM, whose structure is drawn from that of the linear complex filter. The end results are a class of simple, fast, and robust complex filters.

The organization of the paper is as follows. In Section II, the complex WM filters and their statistical properties are introduced. In Section III, a least mean square (LMS) optimization is presented. Applications and simulation results are presented in Section IV, and Section V is devoted to the conclusions.

II. Complex WM Filters

The weighting strategy is essential to filtering operations. Many communications related applications, such as matched filtering, equalization, beamforming, etc., require filtering structures admitting complex-valued weights. For linear filters, there are no difficulties in obtaining the optimal weights. However, due to the nonlinear nature of the median operation, the optimal complex weight design for median-type filters has not been explored in the literature to our best knowledge, and even the meaning of complex weighting itself is vague. In this section, based on two different interpretations of complex weighting, we propose a set of complex WM filter structures that can fully exploit its power and still keep the advantages inherited from univariate medians. The simplest approach to attain complex WM filtering is to perform marginal operations where the real component of the weights $W_R\,|_{i=1}^{N}$ affect the real part of the samples $X_R\,|_{i=1}^{N}$ and the imaginary component of the weights $W_I\,|_{i=1}^{N}$ affect the imaginary part of the samples $X_I\,|_{i=1}^{N}$. This approach referred to as *marginal* complex WM filter outputs:

$$\begin{aligned}\hat{\beta}_{\text{marginal}} = {} & \text{MEDIAN}\left(|W_{R_i}| \diamond \text{sgn}(W_{R_i})\, X_{R_i}\ \big|_{i=1}^{N}\right) \\ & + j\,\text{MEDIAN}\left(|W_{I_i}| \diamond \text{sgn}(W_{I_i})\, X_{I_i}\ \big|_{i=1}^{N}\right)\end{aligned} \tag{8}$$

where $\diamond$ is the replication operator defined as $W \diamond X = \overbrace{X, X, \ldots, X}^{W \text{ times}}$, and the real and imaginary components are decoupled. In general, the WM can be computed without replicating the sample data according to the corresponding weights, as this increases the computational complexity. A more efficient method to find the WM is shown next, which not only is attractive from a computational perspective, but it also admits positive real-valued weights.

1) Calculate the threshold $T_0 = (1/2)\sum_{i=1}^{N} W_i$.
2) Sort the samples in the observation vector $\mathbf{X}(n)$.
3) Sum the concomitant weights[2] of the sorted samples beginning with the maximum sample and continuing down in order.
4) The output is the sample whose weight causes the sum to become $\geq T_0$.

[2]Represent the input samples and their corresponding weights as pairs of the form (X_i, W_i). If the pairs are ordered by their X variates, then the value of W associated with $X_{(m)}$, which is denoted by $W_{(m)}$, is referred to as the *concomitant of the mth-order statistic* [7].

The definition in (8) assumes that the real and imaginary components of the input samples are independent. On the other hand, if the real and imaginary domains are correlated, better performance is attainable by mutually *coupling* the real and imaginary components of the signal and weights.

In the context of filtering, weights are used to emphasize or de-emphasize the input samples based on the temporal and ordinal correlation or any other information contained in the signal. Moreover, not only to indicate the reliability of samples, the weights can also be used to change the original data pattern into an appropriate one. Consider the mean operation with complex-valued weights $W_i = |W_i|e^{j\theta_i}|_{i=1}^N$,

$$\begin{aligned}\bar{\beta} &= \text{MEAN}(W_1^* \cdot X_1, W_2^* \cdot X_2, \ldots, W_N^* \cdot X_N) \\ &= \frac{1}{N}\sum_{i=1}^{N} |W_i| \cdot e^{-j\theta_i} X_i. \end{aligned} \tag{9}$$

The simple manipulation used in (9) reveals that the weights have two roles in the weighted mean operation, i.e., first their phases are coupled into the samples changing them into a new group of *phased* samples, and then, the magnitudes of the weights are applied. The process of decoupling the phase from the weight and merging it to the associated input sample is called *phase coupling*. The definition of the *phase-coupled* complex WM filter follows by analogy.

A. Phase-Coupled Complex WM Filter

Given the complex valued samples $X_1, X_2, \ldots X_N$ and the complex valued weights $W_i = |W_i|e^{j\theta_i}, i = 1, \ldots, N$, the output of the phase-coupled complex WM is defined as

$$\hat{\beta} = \arg\inf_{\beta} \sum_{i=1}^{N} |W_i| \left| e^{-j\theta_i} X_i - \beta \right|. \tag{10}$$

This definition of the complex WM delivers a rich class of complex median filtering structures. The solution to (10), however, suffers from computational complexity as the cost function must be searched for its minimum. Any one of the already mentioned suboptimal approximations, i.e., assume that the output $\hat{\beta}$ is one of the phase-coupled input samples or split the problem into real and imaginary parts, arise as effective ways to reduce the complexity. The first approximation referred to as the *selection phase-coupled* complex WM reduces (10) to

$$\hat{\beta} = \arg\min_{\beta \in \{e^{-j\theta_i} X_i\}} \sum_{i=1}^{N} |W_i| \left| e^{-j\theta_i} X_i - \beta \right|. \tag{11}$$

Since $\hat{\beta}$ is confined to be one of the phase-coupled inputs, this filter is intuitively desirable when very sensitive information is carried by the phase of samples and weights. However, the computation of (11) requires the evaluation of the cost function for each one of the phase-coupled input samples and, thus, may be not suitable for fast applications. The following definitions provide efficient and fast complex-valued WM filter structures.

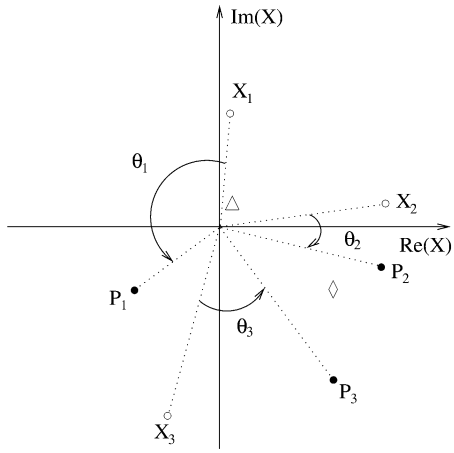

Fig. 1. Marginal phase-coupled CWM illustration. "○:" original samples."·:" phase-coupled samples. "△:" marginal median output. "◇:" marginal phase-coupled median output.

B. Marginal Phase-Coupled Complex WM Filter

The marginal phase-coupled complex WM filter reduces the output in (10) to the following two real-valued WMs:

$$\begin{aligned}\hat{\beta}_R &= \arg\inf_{\beta_R} \sum_{i=1}^{N} |W_i| \left| \text{Re}\left\{e^{-j\theta_i} X_i\right\} - \beta_R \right| \\ &= \text{MEDIAN}\left(|W_i| \diamond \text{Re}\left\{e^{-j\theta_i} X_i\right\} \Big|_{i=1}^{N} \right) \end{aligned} \tag{12}$$

$$\begin{aligned}\hat{\beta}_I &= \arg\inf_{\beta_I} \sum_{i=1}^{N} |W_i| \left| \text{Im}\left\{e^{-j\theta_i} X_i\right\} - \beta_I \right| \\ &= \text{MEDIAN}\left(|W_i| \diamond \text{Im}\left\{e^{-j\theta_i} X_i\right\} \Big|_{i=1}^{N} \right) \end{aligned} \tag{13}$$

where $\text{Re}\{\cdot\}$ and $\text{Im}\{\cdot\}$ denote real and imaginary part, respectively, and the filter output is $\hat{\beta} = \hat{\beta}_R + j\hat{\beta}_I$.

To help understand this definition better, a simple example is given in Fig. 1. Three complex-valued samples X_1, X_2, X_3 and three complex-valued weights in the unit circle W_1, W_2, W_3 are arbitrarily chosen. The phase-coupled samples P_1, P_2, P_3 are plotted to show the effect of phase coupling. The weights are not directly shown on the figure, but their phases θ_1, θ_2, and $, \theta_3$ are shown as the angles between the original and altered samples. In addition, since the marginal phase-coupled complex WM filter outputs one of the real and imaginary parts of the phase-coupled samples, the filter does not necessarily select one of the phase-coupled inputs, which gives it more flexibility than the selection phase-coupled complex WM filter.

C. Real-Imaginary Coupled Complex WM Filter

In phase coupling, the phases of the weights modify the phases of the input samples, and the norms of the weights perform the smoothing operation in the real and imaginary domains independently. As an alternative, we can use the complex-valued weights to exploit the coupling characteristics between the real and imaginary parts of the input signal. These characteristics are shown in the computation of the complex linear filter. Letting $\mathbf{W} = [W_1, W_2, \ldots, W_N]^T$ and

$\mathbf{X} = [X_1, X_2, \ldots, X_N]^T$, the output of the complex linear filter is

$$\begin{aligned}\bar{\beta} &= \mathbf{W}^H\mathbf{X} = \left(\mathbf{W}_R^T - j\mathbf{W}_I^T\right)\cdot(\mathbf{X}_R + j\mathbf{X}_I) \\ &= \left(\mathbf{W}_R^T\mathbf{X}_R + \mathbf{W}_I^T\mathbf{X}_I + j\mathbf{W}_R^T\mathbf{X}_I - j\mathbf{W}_I^T\mathbf{X}_R\right) \quad (14)\end{aligned}$$

where $\mathbf{W}_R = \mathrm{Re}\{\mathbf{W}\}, \mathbf{W}_I = \mathrm{Im}\{\mathbf{W}\}, \mathbf{X}_I = \mathrm{Im}\{\mathbf{X}\}, \mathbf{X}_R = \mathrm{Re}\{\mathbf{X}\}$. Defining the following vectors $\mathbf{W}_{RI}^T = [\mathbf{W}_R^T \mid \mathbf{W}_I^T], \mathbf{X}_{RI}^T = [\mathbf{X}_R^T \mid \mathbf{X}_I^T], \mathbf{X}_{IR-}^T = [\mathbf{X}_I^T \mid -\mathbf{X}_R^T]$, the complex linear filtering structure can be rewritten as

$$\bar{\beta} = \mathbf{W}^H\mathbf{X} = \mathbf{W}_{RI}^T\mathbf{X}_{RI} + j\mathbf{W}_{RI}^T\mathbf{X}_{IR-}. \quad (15)$$

Thus, the complex linear filter can be split into two real linear filtering structures. This representation is very convenient since the vector $\mathbf{W}_{RI}^T$ is used in both real-valued filtering operations. Additionally, the two data vectors $\mathbf{X}_{RI}$ and $\mathbf{X}_{IR-}$ are created from the original input data vector, which is not computationally expensive. The linear complex filtering representation in (15) motivates the following definition of the complex WM operation, namely, the *real-imaginary coupled* complex WM:

$$\begin{aligned}\hat{\beta} &= \mathrm{MEDIAN}\left(\mathbf{W}_{RI}^T \diamond \mathbf{X}_{RI}\right) + j\,\mathrm{MEDIAN}\left(\mathbf{W}_{RI}^T \diamond \mathbf{X}_{IR-}\right) \\ &= \mathrm{MEDIAN}\left(|W_{R_i}| \diamond \mathrm{sgn}(W_{R_i})\,X_{R_i} \;\big|_{i=1}^{N}\right. \\ &\quad \left.|W_{I_i}| \diamond \mathrm{sgn}(W_{I_i})\,X_{I_i} \;\big|_{i=1}^{N}\right) \\ &\quad + j\,\mathrm{MEDIAN}\left(|W_{R_i}| \diamond \mathrm{sgn}(W_{R_i})\,X_{I_i} \;\big|_{i=1}^{N}\right. \\ &\quad \left.|W_{I_i}| \diamond -\mathrm{sgn}(W_{I_i})\,X_{R_i} \;\big|_{i=1}^{N}\right) \quad (16)\end{aligned}$$

where $W_{R_i} = \mathrm{Re}\{W_i\}, W_{I_i} = \mathrm{Im}\{W_i\}$, $X_{R_i} = \mathrm{Re}\{X_i\}$, and $X_{I_i} = \mathrm{Im}\{X_i\}$ for $i = 1, 2, \ldots, N$.

Three important characteristics provide a strong support for this definition. First, the sample vectors $\mathbf{X}_{RI}$ and $\mathbf{X}_{IR-}$ are intrinsically coupled in the complex space. This facilitates to perform the optimization of the filter in a joint (real and imaginary components) manner. Second, the computation in (16) does not require any suboptimal implementation since it consists of two real-valued WM operations that are known to be fast. Last, the definition in (16) reduces to the real-valued WM filter when the samples and weights are real-valued.

Fig. 2 depicts the effect of complex weighting on the filters introduced in this paper, namely, phase-coupled complex WM, selection phase-coupled complex WM, marginal phase-coupled complex WM, and real-imaginary coupled complex WM filters. Fig. 2(a) shows the distribution in the complex plane of the input samples $X_i\,|_{i=1}^{8}$ and the associated weights $W_i\,|_{i=1}^{8}$. Additionally, a second set of weights where the first four weights $W_i\,|_{i=1}^{4}$ are modified is shown in order to study the effect of the complex weighting on the contours of the cost functions and on the outputs of the complex WM filters. Fig. 2(b) shows both the original and modified set of phase-coupled samples $P_i\,|_{i=1}^{8}$ and the effect of the complex weighting on the output of the phased coupled WM filter and the contours of its cost function. The solid line contours depicted correspond to the original set of weights, and the dashed-line contours correspond to the modified set of

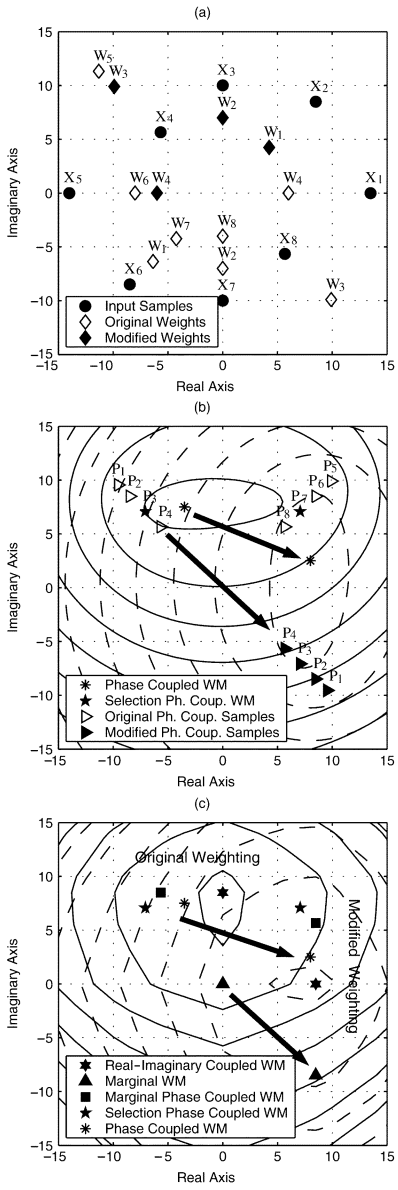

Fig. 2. Weighting effect on the contours of the cost functions and outputs of the complex WM filters. (a) Distribution of input samples and original and modified weights. (b) Cost function contours and output for phase-coupled complex WM and outputs of selection phase-coupled complex WM for both original and modified weighting. (c) Cost function contours of real-imaginary complex WM and comparison of complex WM filter outputs for both original and modified weighting.

weights. Fig. 2(c) has the contours of the real-imaginary coupled complex WM filter and summarizes the effect of complex weighting on all the complex WM filter outputs. As the arrows show, all the outputs follow the same trend as the set of weights $W_i\,|_{i=1}^{4}$ changes, except for the marginal complex WM output, which does not follow the rotation tendency exhibited by the other filter outputs. It is clear from this example that in general, all these complex WM filters provide different outputs for the same set of input samples and weights. Therefore, when one of these filters is desired for a nonlinear signal processing application, it is important to take into account the characteristics of that specific application in order to pick the filter that makes the best fit. Some examples on how to choose the proper filter will be given in Section IV.

III. Optimization

In this section, we first extend threshold decomposition TD into the complex domain and then use it to derive adaptive algorithms for both marginal phase-coupled and real-imaginary coupled complex WM filters in the minimum mean square error sense.

A. Complex Threshold Decomposition

Threshold decomposition is an important tool in the analysis of WMs. It was first introduced in [8] for signals taking on positive integer values. Later, threshold decomposition was extended to the real domain [4]. For any real-valued sample X_i, its real threshold decomposition (RTD) representation is

$$X_i = \frac{1}{2}\int_{-\infty}^{\infty} x_i^q \,\mathrm{d}q \tag{17}$$

where $-\infty < q < \infty$, and

$$x_i^q = \mathrm{sgn}(X_i - q) = \begin{cases} 1, & \text{if } X_i \geq q \\ -1, & \text{if } X_i < q. \end{cases} \tag{18}$$

Thus, given the samples $\{X_i\,|_{i=1}^N\}$ and the real-valued weights $\{W_i\,|_{i=1}^N\}$, the WM filter can be expressed as

$$\begin{aligned} Y &= \mathrm{MED}\left(|W_i| \diamond \mathrm{sgn}(W_i)X_i\,\big|_{i=1}^N\right) \\ &= \mathrm{MED}\left(|W_i| \diamond \frac{1}{2}\int_{-\infty}^{\infty} \mathrm{sgn}(\mathrm{sgn}(W_i) \right. \\ &\qquad \left. \times\, X_i - q)\,\mathrm{d}q\,\big|_{i=1}^N\right). \end{aligned} \tag{19}$$

Expression (19) is the median operation of a set of weighted integrals that represent the threshold decomposition of the samples $X_i\,|_{i=1}^N$. Note that the same result is obtained if the WM of these functions, at each value of q, is taken first, and the resultant signal is integrated over the variable q. Thus, the order of the integral and the median operator can be interchanged without affecting the result.[3] This leads to

$$Y = \frac{1}{2}\int_{-\infty}^{\infty} \mathrm{MED}\left(|W_i| \diamond s_i^q\,\big|_{i=1}^N\right)\mathrm{d}q \tag{20}$$

where $S_i = \mathrm{sgn}(W_i)X_i, \mathbf{S} = [S_1, S_2, \ldots, S_N]^T$, $s_i^q = \mathrm{sgn}(S_i - q)$, and $\mathbf{S}^q = [s_1^q, s_2^q, \ldots s_N^q]^T$. Since the samples of the median filter inside the integral in (20) are either 1 or -1 for each q, this median operation can be efficiently calculated as $\mathrm{sgn}(\mathbf{W}_a^T\mathbf{S}^q)$, where the elements of the new vector $\mathbf{W}_a^T$ are given by $|W_i|\,|_{i=1}^N$. Equation (20) can be written as

$$Y = \frac{1}{2}\int_{-\infty}^{\infty} \mathrm{sgn}\big(\mathbf{W}_a^T\mathbf{S}^q\big)\,\mathrm{d}q. \tag{21}$$

Therefore, the extension of the threshold decomposition representation to the complex field can be naturally carried out as

$$\begin{aligned} X = \frac{1}{2}\int_{-\infty}^{\infty} \mathrm{sgn}(\mathrm{Re}\{X\} - q)\,\mathrm{d}q \\ + j\frac{1}{2}\int_{-\infty}^{\infty} \mathrm{sgn}(\mathrm{Im}\{X\} - p)\,\mathrm{d}p \end{aligned} \tag{22}$$

where RTD is applied onto real and imaginary parts of the complex signal X separately.

[3]Refer to [4] for details.

B. Optimal Marginal Phase-Coupled Complex WM

The real and imaginary parts of the output of the marginal phase-coupled complex WM in (12) and (13) are two separate real median operations, and thus, the complex-valued threshold decomposition in (22) can be directly applied. Given the complex-valued samples $\{X_i\,|_{i=1}^N\}$, the complex-valued weights $\{|W_i|e^{-j\theta_i}\,|_{i=1}^N\}$ define $P_i = e^{-j\theta_i}X_i\,|_{i=1}^N$ as the phase-coupled input samples and its real and imaginary parts as $P_{R_i} = \mathrm{Re}\{P_i\}, P_{I_i} = \mathrm{Im}\{P_i\}$. Additionally

$$\begin{aligned} p_{R_i}^s &= \mathrm{sgn}(P_{R_i} - s), \quad \mathbf{P}_R^s = \left[p_{R_1}^s, p_{R_2}^s, \ldots, p_{R_N}^s\right]^T \\ p_{I_i}^r &= \mathrm{sgn}(P_{I_i} - r), \quad \mathbf{P}_I^r = \left[p_{I_1}^r, p_{I_2}^r, \ldots, p_{I_N}^r\right]^T. \end{aligned}$$

Similar to the RTD representation of WM in (21), the complex-valued threshold decomposition for the marginal phase-coupled complex WM can be implemented as

$$\begin{aligned} \hat{\beta}(n) &= \mathrm{MED}\left(|W_i| \diamond P_{R_i}\,\big|_{i=1}^N\right) \\ &\quad + j\,\mathrm{MED}\left(|W_i| \diamond P_{I_i}\,\big|_{i=1}^N\right) \\ &= \mathrm{MED}\left(|W_i| \diamond \frac{1}{2}\int_{-\infty}^{\infty} p_{R_i}^s\,\mathrm{d}s\,\big|_{i=1}^N\right) \\ &\quad + j\,\mathrm{MED}\left(|W_i| \diamond \frac{1}{2}\int_{-\infty}^{\infty} p_{I_i}^r\,\mathrm{d}r\,\big|_{i=1}^N\right) \\ &= \frac{1}{2}\int_{-\infty}^{\infty} \mathrm{MED}\left(|W_i| \diamond p_{R_i}^s\,\big|_{i=1}^N\right)\mathrm{d}s \\ &\quad + j\frac{1}{2}\int_{-\infty}^{\infty} \mathrm{MED}\left(|W_i| \diamond p_{I_i}^r\,\big|_{i=1}^N\right)\mathrm{d}r \\ &= \frac{1}{2}\left\{\int_{-\infty}^{\infty} \mathrm{sgn}\big(\mathbf{W}_a^T\mathbf{P}_R^s\big)\,\mathrm{d}s \right. \\ &\quad \left. + \,j\int_{-\infty}^{\infty} \mathrm{sgn}\big(\mathbf{W}_a^T\mathbf{P}_I^r\big)\,\mathrm{d}r\right\}. \end{aligned} \tag{23}$$

Assume that the observed process $\{X(n)\}$ and the desired process $\{\beta(n)\}$ are jointly stationary. The filter output $\hat{\beta}(n)$ estimating the desired signal $\beta(n)$ is given in (23). Under the mean square error (MSE) criterion, the cost function to minimize is

$$\begin{aligned} J(n) &= \mathrm{E}\{|\beta(n) - \hat{\beta}(n)|^2\} \\ &= \mathrm{E}\left\{\left|\frac{1}{2}\int_{-\infty}^{\infty} \left(\mathrm{sgn}(\beta_R - s) - \mathrm{sgn}\big(\mathbf{W}_a^T\mathbf{P}_R^s\big)\right)\mathrm{d}s \right.\right. \\ &\quad \left.\left. + \,j\frac{1}{2}\int_{-\infty}^{\infty} \left(\mathrm{sgn}(\beta_I - r) - \mathrm{sgn}\big(\mathbf{W}_a^T\mathbf{P}_I^r\big)\right)\mathrm{d}r\right|^2\right\} \\ &= \frac{1}{4}\mathrm{E}\left\{\left(\int_{-\infty}^{\infty} e_R^s\,\mathrm{d}s\right)^2 + \left(\int_{-\infty}^{\infty} e_I^r\,\mathrm{d}r\right)^2\right\} \end{aligned} \tag{24}$$

where $\beta_R = \mathrm{Re}\{\beta(n)\}, \beta_I = \mathrm{Im}\{\beta(n)\}, e_R = \mathrm{Re}\{\beta(n) - \hat{\beta}(n)\}, e_I = \mathrm{Im}\{\beta(n) - \hat{\beta}(n)\}$. Utilizing the relationship be-

tween the complex gradient vector ∇J and the conjugate derivative $\partial J/\partial \mathbf{W}^*$ [9], we have

$$\begin{aligned}\nabla J(n) &= 2\frac{\partial J(\mathbf{W})}{\partial \mathbf{W}^*} \\ &= -\mathrm{E}\left\{\left(\int_{-\infty}^{\infty} e_R^s \mathrm{d}s\right)\left(\int_{-\infty}^{\infty} \frac{\partial}{\partial \mathbf{W}^*}\operatorname{sgn}\left(\mathbf{W}_a^T\mathbf{P}_R^s\right)\mathrm{d}s\right)\right. \\ &\quad \left. + \left(\int_{-\infty}^{\infty} e_I^r \,\mathrm{d}r\right)\left(\int_{-\infty}^{\infty} \frac{\partial}{\partial \mathbf{W}^*}\operatorname{sgn}\left(\mathbf{W}_a^T\mathbf{P}_I^r\right)\mathrm{d}r\right)\right\} \\ &= -2\mathrm{E}\left\{e_R \cdot \left(\int_{-\infty}^{\infty} \frac{\partial}{\partial \mathbf{W}^*}\operatorname{sgn}\left(\mathbf{W}_a^T\mathbf{P}_R^s\right)\mathrm{d}s\right)\right. \\ &\quad \left. + e_I \cdot \left(\int_{-\infty}^{\infty} \frac{\partial}{\partial \mathbf{W}^*}\operatorname{sgn}\left(\mathbf{W}_a^T\mathbf{P}_I^r\right)\mathrm{d}r\right)\right\}. \end{aligned} \tag{25}$$

To take the derivatives needed in (25), the sign function is approximated by a differentiable one to circumvent the inconvenience of having a Dirac impulse term in further analysis. The chosen substitute is the hyperbolic tangent function $\operatorname{sgn}(x) \approx \tanh(x) = (e^x - e^{-x})/(e^x + e^{-x})$ and its derivative $(d/dx)\tanh(x) = \operatorname{sech}^2(x) = (4)/((e^x + e^{-x})^2)$. Thus, $(\partial)/(\partial \mathbf{W}^*)\operatorname{sgn}(\mathbf{W}_a^T\mathbf{P}_R^s) \approx \operatorname{sech}^2(\mathbf{W}_a^T\mathbf{P}_R^s)(\partial)/(\partial \mathbf{W}^*)(\mathbf{W}_a^T\mathbf{P}_R^s)$. Furthermore, the derivative with respect to only one weight is

$$\begin{aligned}&\frac{\partial}{\partial W_i^*}\operatorname{sgn}\left(\mathbf{W}_a^T\mathbf{P}_R^s\right) \\ &\quad \approx \operatorname{sech}^2\left(\mathbf{W}_a^T\mathbf{P}_R^s\right)\frac{\partial}{\partial W_i^*}\left(|W_i|p_{R_i}^s\right) \\ &\quad = \operatorname{sech}^2\left(\mathbf{W}_a^T\mathbf{P}_R^s\right)\left(\frac{\partial |W_i|}{\partial W_i^*}p_{R_i}^s + |W_i|\frac{\partial p_{R_i}^s}{\partial W_i^*}\right). \end{aligned} \tag{26}$$

In addition, given that

$$\frac{\partial P_{R_i}}{\partial W_i^*} = \frac{1}{2}\frac{\partial}{\partial W_i^*}(P_i + P_i^*) = \frac{1}{2}\frac{1}{|W_i^*|}e^{j\theta_i}jP_{I_i}$$

we have

$$\begin{aligned}\frac{\partial}{\partial W_i^*}\operatorname{sgn}\left(\mathbf{W}_a^T\mathbf{P}_I^r\right) \approx \frac{1}{2}&\operatorname{sech}^2\left(\mathbf{W}_a^T\mathbf{P}_I^r\right)e^{j\theta_i} \\ &\times \left(p_{I_i}^r - \operatorname{sech}^2\left(P_{I_i} - r\right)jP_{R_i}\right) \end{aligned} \tag{27}$$

and similarly

$$\begin{aligned}\frac{\partial}{\partial W_i^*}\operatorname{sgn}\left(\mathbf{W}_a^T\mathbf{P}_R^s\right) \approx \frac{1}{2}&\operatorname{sech}^2\left(\mathbf{W}_a^T\mathbf{P}_R^s\right)e^{j\theta_i} \\ &\times \left(p_{R_i}^s + \operatorname{sech}^2(P_{R_i} - s)jP_{I_i}\right). \end{aligned} \tag{28}$$

Integrating both sides

$$\begin{aligned}&\int_{-\infty}^{\infty}\frac{\partial}{\partial W_i^*}\operatorname{sgn}\left(\mathbf{W}_a^T\mathbf{P}_R^s\right)\mathrm{d}s \\ &\quad \approx \frac{1}{2}e^{j\theta_i}\int_{-\infty}^{\infty}\operatorname{sech}^2\left(\mathbf{W}_a^T\mathbf{P}_R^s\right)P_{R_i}^s\,\mathrm{d}s \\ &\qquad + \frac{1}{2}e^{j\theta_i}jP_{I_i}\int_{-\infty}^{\infty}\operatorname{sech}^2\left(\mathbf{W}_a^T\mathbf{P}_R^s\right)\operatorname{sech}^2\left(P_{R_i} - s\right)\mathrm{d}s. \end{aligned} \tag{29}$$

The second integral can be expanded as follows:

$$\begin{aligned}&\int_{-\infty}^{\infty}\operatorname{sech}^2\left(\mathbf{W}_a^T\mathbf{P}_R^s\right)\operatorname{sech}^2\left(P_{R_i} - s\right)\mathrm{d}s \\ &\quad = \operatorname{sech}^2\left(\mathbf{W}_a^T\mathbf{P}_R^{P_{R_{(1)}}^-}\right)\int_{-\infty}^{P_{R_{(1)}}}\operatorname{sech}^2\left(P_{R_i} - s\right)\mathrm{d}s \\ &\qquad + \sum_{k=1}^{N-1}\operatorname{sech}^2\left(\mathbf{W}_a^T\mathbf{P}_R^{P_{R_{(k+1)}}^-}\right) \\ &\qquad \times \int_{P_{R_{(k)}}}^{P_{R_{(k+1)}}}\operatorname{sech}^2\left(P_{R_i} - s\right)\mathrm{d}s \\ &\qquad + \operatorname{sech}^2\left(\mathbf{W}_a^T\mathbf{P}_R^{P_{R_{(N)}}^+}\right)\int_{P_{R_{(N)}}}^{\infty}\operatorname{sech}^2\left(P_{R_i} - s\right)\mathrm{d}s \end{aligned} \tag{30}$$

and remembering that

$$\int \operatorname{sech}^2(x)\,\mathrm{d}x = \int \mathrm{d}\{\tanh(x)\}, \tag{31}$$

$$\begin{aligned}&\int_{-\infty}^{\infty}\operatorname{sech}^2\left(\mathbf{W}_a^T\mathbf{P}_R^s\right)\operatorname{sech}^2\left(P_{R_i} - s\right)\mathrm{d}s \\ &\quad = \operatorname{sech}^2\left(\mathbf{W}_a^T\mathbf{P}_R^{P_{R_{(1)}}^-}\right)\tanh\left(P_{R_i} - s\right)\Big|_{-\infty}^{P_{R_{(1)}}} \\ &\qquad + \sum_{k=1}^{N-1}\operatorname{sech}^2\left(\mathbf{W}_a^T\mathbf{P}_R^{P_{R_{(k+1)}}^-}\right)\tanh\left(P_{R_i} - s\right)\Big|_{P_{R_{(k)}}}^{P_{R_{(k+1)}}} \\ &\qquad + \operatorname{sech}^2\left(\mathbf{W}_a^T\mathbf{P}_R^{P_{R_{(N)}}^+}\right)\tanh\left(P_{R_i} - s\right)\Big|_{P_{R_{(N)}}}^{\infty}. \end{aligned} \tag{32}$$

Now, $\tanh(x)$ can be replaced with $\operatorname{sign}(x)$. As a result, all terms involving $\operatorname{sign}(P_{R_i} - s)$ in the previous equation will be zero, except the one when $P_{R_i} = P_{R_{(k)}}$. In this case, $\operatorname{sign}(P_{R_i} - s)\big|_{P_{R_{(k)}}}^{P_{R_{(k+1)}}} = 2$.

On the other hand, when $P_{R_i} = \hat{\beta}_R$, the product $\mathbf{W}_a^T\mathbf{P}_R^s$ is approximately zero. In this case, $\operatorname{sech}^2(\mathbf{W}_a^T\mathbf{P}_R^s) \approx 1$, and since this is the largest contributor to the sum in (33), all the other terms can be omitted. All this approximation results in

$$\begin{aligned}&\int_{-\infty}^{\infty}\frac{\partial}{\partial W_i^*}\operatorname{sgn}\left(\mathbf{W}_a^T\mathbf{P}_R^s\right)\mathrm{d}s \\ &\quad \approx \frac{1}{2}e^{j\theta_i}\left(\operatorname{sgn}\left(P_{R_i} - \hat{\beta}_R\right) + 2jP_{I_i}\delta\left(P_{R_i} - \hat{\beta}_R\right)\right) \end{aligned} \tag{33}$$

$$\begin{aligned}&\int_{-\infty}^{\infty}\frac{\partial}{\partial W_i^*}\operatorname{sgn}\left(\mathbf{W}_a^T\mathbf{P}_I^r\right)\mathrm{d}r \\ &\quad \approx \frac{1}{2}e^{j\theta_i}\left(\operatorname{sgn}\left(P_{I_i} - \hat{\beta}_I\right) + 2jP_{R_i}\delta\left(P_{I_i} - \hat{\beta}_I\right)\right) \end{aligned} \tag{34}$$

leading to the following weight update equation:

$$\begin{aligned} W_i(n+1) &= W_i(n) + \mu\{-\nabla J(n)\} \\ &\approx W_i(n) + \mu e^{j\theta_i}\Big\{e_R(n)\text{sgn}\Big(P_{R_i}(n) - \hat{\beta}_R(n)\Big) \\ &\quad + e_I(n)\text{sgn}\Big(P_{I_i}(n) - \hat{\beta}_I(n)\Big) \\ &\quad + 2je_R(n)\left(P_{I_i}(n)\delta\left(P_{R_i}(n) - \hat{\beta}_R(n)\right)\right. \\ &\quad \left. + 2je_I(n)\left(P_{R_i}(n)\delta\left(P_{I_i}(n) - \hat{\beta}_I(n)\right)\right)\Big\}. \end{aligned} \tag{35}$$

C. Optimal Real-Imaginary Coupled Complex WM

It is desired to find the optimum set of coupled real-valued weights $\mathbf{W}_{RI}$ needed in the *real-imaginary coupled* complex WM in the minimum squared error sense. A least mean square (LMS) algorithm for the adaptation of the weights is developed. The recursive equation can be written as

$$W_{RI_k}(n+1) = W_{RI_k}(n) + \mu\{-\nabla J(n)\} \tag{36}$$

where $\nabla J(n) = \partial J(n)/\partial W_{RI_k}$, and $J(n)$ is the mean squared error cost function defined as

$$\begin{aligned} J(n) &= E[|\beta(n) - \hat{\beta}(n)|^2] \\ &= E[(\beta_R(n) - \hat{\beta}_R(n))^2 + (\beta_I(n) - \hat{\beta}_I(n))^2]. \end{aligned} \tag{37}$$

The gradient $\nabla J(n)$ needs to be calculated using instantaneous estimates since the expected values are not available:

$$\begin{aligned} \frac{\partial}{\partial W_{RI_k}} J(n) \approx -2\Bigg[&(\beta_R(n) - \hat{\beta}_R(n))\frac{\partial}{\partial W_{RI_k}}\hat{\beta}_R(n) \\ &+ (\beta_I(n) - \hat{\beta}_I(n))\frac{\partial}{\partial W_{RI_k}}\hat{\beta}_I(n)\Bigg]. \end{aligned} \tag{38}$$

The calculation of the partial derivatives of $\hat{\beta}_R(n)$ and $\hat{\beta}_I(n)$ need the use of threshold decomposition [4] as follows:

$$\begin{aligned} \hat{\beta}_R(n) = \text{MEDIAN}\Bigg(&|W_{RI_i}(n)| \diamond \frac{1}{2}\int_{-\infty}^{\infty} \text{sgn}\big(\text{sgn}\big(W_{RI_i(n)}\big) \\ &\times X_{RI_i}(n) - q\big)\, \mathrm{d}q \,\Big|_{i=1}^{2N}\Bigg). \end{aligned} \tag{39}$$

Since similar arguments are used for the calculation of both terms, the derivative of $\hat{\beta}_R(n)$ will be first found, and then, the derivative of $\hat{\beta}_I(n)$ will be deduced by analogy. Using similar arguments to the ones explained in (20) and (21), (39) can be expressed as

$$\begin{aligned} \hat{\beta}_R(n) &= \frac{1}{2}\int_{-\infty}^{\infty} \text{MEDIAN}\left(|W_{RI_i}(n)| \diamond \text{sgn}(\text{sgn}(W_{RI_i}(n))\right. \\ &\quad \left. \times\ X_{RI_i}(n) - q)\ \Big|_{i=1}^{2N}\right)\mathrm{d}q \\ &= \frac{1}{2}\int_{-\infty}^{\infty} \text{sgn}\big(\mathbf{W}_{RI_a}^T\mathbf{S}_{RI}^q\big)\,\mathrm{d}q \end{aligned} \tag{40}$$

where the elements of the vectors $\mathbf{W}_{RI_a}^T$ and $\mathbf{S}_{RI}^q$ are given by $W_{RI_{ai}} = |W_{RI_i}(n)|\,|_{i=1}^{2N}$ and $s_{RI_i}^q = \text{sgn}(\text{sgn}(W_{RI_i}(n))\, X_{RI_i}(n) - q)\,|_{i=1}^{2N}$, respectively.

The derivative of $\hat{\beta}_R(n)$ is equal to

$$\frac{\partial\hat{\beta}_R(n)}{\partial W_{RI_i}} = \int_{-\infty}^{\infty} \delta\left(\mathbf{W}_{RI_a}^T\mathbf{S}_{RI}^q\right)\frac{\partial}{\partial W_{RI_i}}\left(\mathbf{W}_{RI_a}^T\mathbf{S}_{RI}^q\right)\mathrm{d}q \tag{41}$$

where it can be shown that

$$\frac{\partial\mathbf{W}_{RI_a}^T\mathbf{S}_{RI}^q}{\partial W_{RI_i}} = \text{sgn}(W_{RI_i})\,\text{sgn}(\text{sgn}(W_{RI_i})\,X_{RI_i}(n) - q). \tag{42}$$

The unit impulse function in (41) is nonzero only when $\mathbf{W}_{RI_a}^T\mathbf{S}_{RI}^q = 0$. In addition, the value of $\mathbf{W}_{RI_a}^T\mathbf{S}_{RI}^q$ that is closest to zero is reached when $q = \hat{\beta}_R(n)$, i.e., when q is equal to the WM output. Strictly speaking, the term $\mathbf{W}_{RI_a}^T\mathbf{S}_{RI}^{\hat{\beta}_R(n)}$ cannot be guaranteed to be equal to zero, therefore nulling the LMS update at time n. Then, this LMS algorithm would wait until the condition $\mathbf{W}_{RI_a}^T\mathbf{S}_{RI}^{\hat{\beta}_R(n)} = 0$ is met to update the weights W_{RI_a}. However, to simplify the algorithm, (41) is approximated as

$$\frac{\partial\hat{\beta}_R(n)}{\partial W_{RI_i}} \approx \text{sgn}(W_{RI_i})\,\text{sgn}\Big(\text{sgn}(W_{RI_i})\,X_{RI_i}(n) - \hat{\beta}_R(n)\Big). \tag{43}$$

Notice that the same result would have been found by approximating the derivative of $\text{sgn}(x)$ with $\text{sech}^2(x)$ and then approximating the integral in (41) by its largest contributing term, as was done in the LMS of the marginal phase-coupled complex WM. We decided to show these two alternative ways to approximate (26) and (41) as we think that together, they provide more insight into the problem.

By analogy, the derivative of $\hat{\beta}_I(n)$ also needed in (38) is given by

$$\frac{\partial\hat{\beta}_I(n)}{\partial W_{RI_i}} \approx \text{sgn}(W_{RI_i})\,\text{sgn}\Big(\text{sgn}(W_{RI_i})\,X_{IR_i^-}(n) - \hat{\beta}_I(n)\Big). \tag{44}$$

Finally, the gradient is calculated as

$$\begin{aligned} &\frac{\partial J(n)}{\partial W_{RI_i}} \\ &\quad \approx -2e_R(n)\text{sgn}(W_{RI_i})\,\text{sgn}\Big(\text{sgn}(W_{RI_i})\,X_{RI_i}(n) - \hat{\beta}_R(n)\Big) \\ &\qquad - 2e_I(n)\text{sgn}(W_{RI_i})\,\text{sgn}\Big(\text{sgn}(W_{RI_i})\,X_{IR_i^-}(n) - \hat{\beta}_I(n)\Big) \end{aligned} \tag{45}$$

where $e_R(n) = \beta_R(n) - \hat{\beta}_R(n)$ and $e_I(n) = \beta_I(n) - \hat{\beta}_I(n)$. After dropping unnecessary scale factors, the desired LMS recursive equation is found to be as follows:

$$\begin{aligned} W_{RI_i}(n+1) = W_{RI_i}(n) + \mu\Big[&e_R(n)\text{sgn}(W_{RI_i}) \\ &\times \text{sgn}\Big(\text{sgn}(W_{RI_i})\,X_{RI_i}(n) - \hat{\beta}_R(n)\Big) \\ &+ e_I(n)\text{sgn}(W_{RI_i})\,\text{sgn}\Big(\text{sgn}(W_{RI_i}) \\ &\times\ X_{IR_i^-}(n) - \hat{\beta}_I(n)\Big)\Big]. \end{aligned} \tag{46}$$

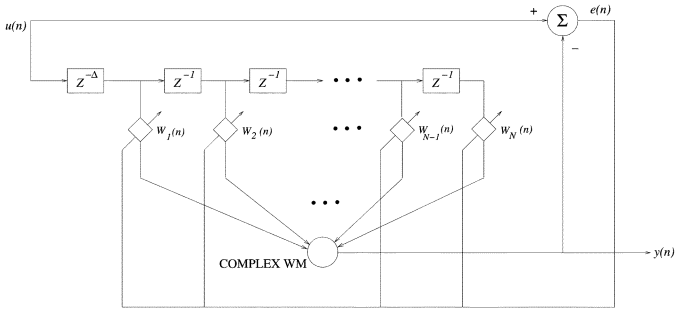

Fig. 3. Block diagram for line enhancer implemented with complex WM filter.

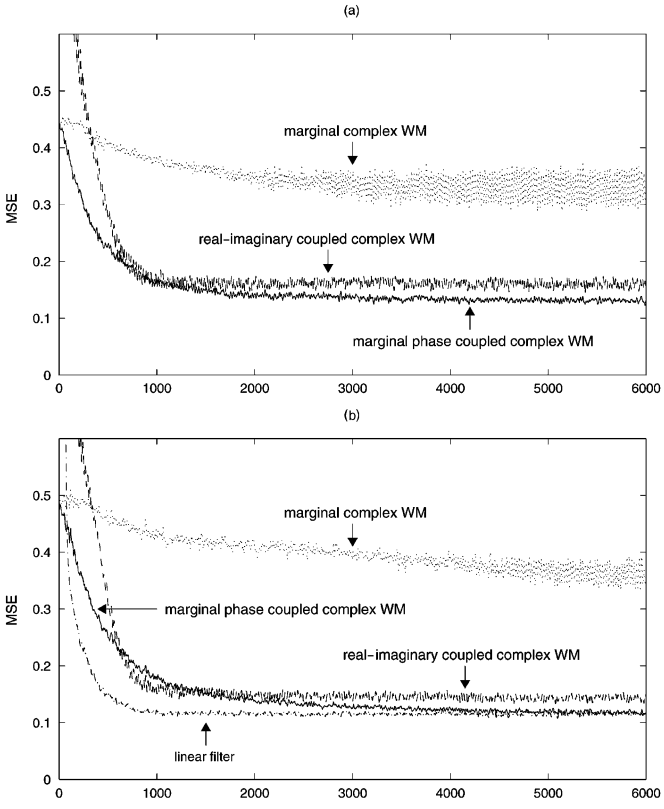

Fig. 4. Learning curves of the LMS algorithm of marginal complex WM, marginal phase-coupled complex WM, and real-imaginary coupled complex WM for line enhancement in α-stable noise with dispersion $\gamma = 0.2$ and $\mu = 0.005$. (a) $\alpha = 1.5$. (b) $\alpha = 2$.

The step-size parameter μ must be chosen properly to achieve the desired convergence rate. Notice that the two update terms in (46) resemble the real-imaginary coupled complex WM characteristics.

IV. Simulations

In this section, the proposed complex WM filters are tested and compared with the classical complex linear filter and to the marginal complex WM filter presented in (8). The first performance evaluation of the filters is carried out within a blind denoising application known as adaptive line-enhancement [9]. This adaptive filter is driven with a delayed version of the input and uses the noisy signal itself as the reference. The goal is to exploit the signal correlation and the noise uncorrelation between the received signal and its shifted version to filter out the noise.

TABLE I
Average MSE Using the LMS for Line Enhancement After Convergence of the Algorithm. ($\mu = 0.005, \gamma = 0.2$)

Filter	$\alpha = 1.3$	$\alpha = 1.5$	$\alpha = 1.7$	$\alpha = 2$
Noisy signal	45.2855	10.1473	3.3539	0.9326
Linear filter	∞	∞	∞	0.1152
Marginal complex WM	0.3759	0.3295	0.3332	0.3682
Real-imaginary coupled complex WM	0.2157	0.1601	0.1434	0.1438
Marginal phase coupled complex WM	0.1929	0.1316	0.1180	0.1154

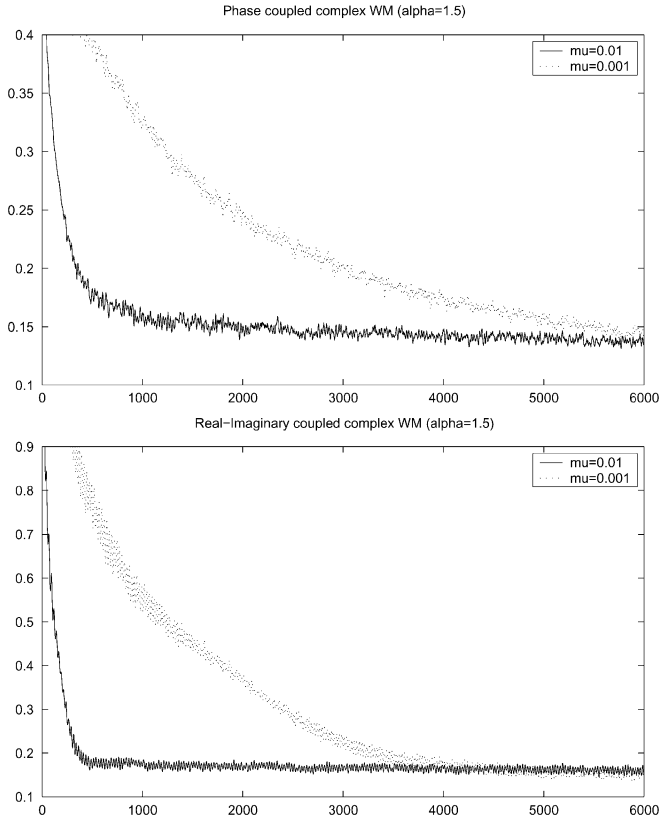

Fig. 5. Learning curves of the LMS algorithm of the marginal phase-coupled complex WM and the real-imaginary coupled complex WM with $\mu = 0.01$ and $\mu = 0.001$ for line enhancement in α-stable noise ($\gamma = 0.2$).

The algorithm also tunes the weights to correct the phase introduced between the filter input and the reference signal. A basic block diagram of a line-enhancer implemented with complex WM filter is shown in Fig. 3.

In the first experiment, the input of an 11-tap line enhancer is a complex exponential contaminated with α-stable noise [10] with dispersion $\gamma = 0.2$, where the value of α runs from 1.3 to 2 (Gaussian noise) to show different levels of noise impulsiveness. The weights of the marginal phase-coupled complex WM filter and the real-imaginary coupled complex WM filter are designed using the previously developed LMS algorithms. In addition, LMS and normalized LMS (NLMS) algorithms are implemented to design a marginal complex WM and a linear complex-valued filter, respectively. Since the marginal complex WM splits the median operation into real and imaginary parts independently, this filter was designed by applying independent LMS algorithms for real-valued WM filters to both real and imaginary domains. The same noisy signal will be filtered using

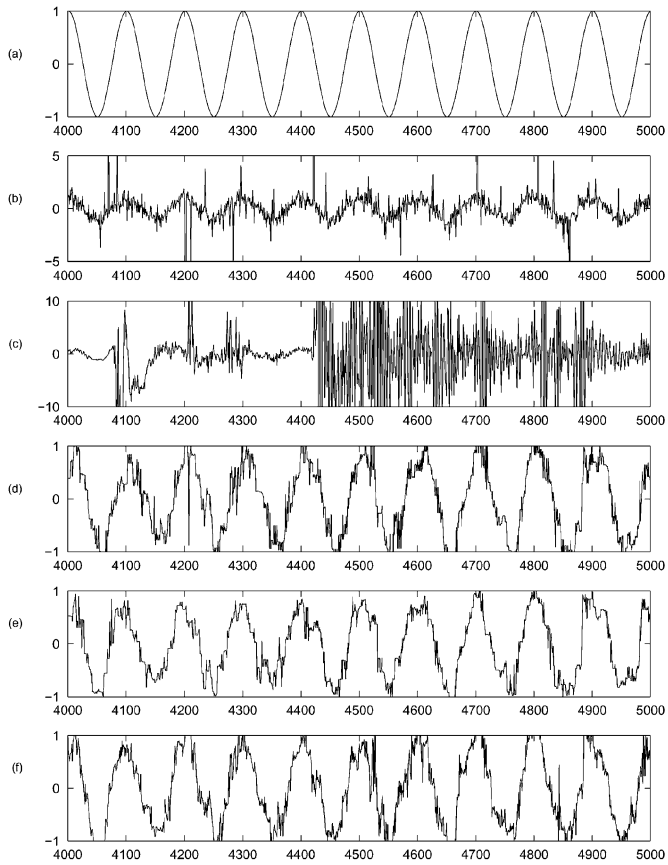

Fig. 6. Real part of the output of the filters for $\alpha = 1.7, \gamma = 0.2$, and $\mu = 0.005$. (a) Original signal. (b) Noisy signal. (c) Linear filter. (d) Marginal complex WM. (e) Real-imaginary coupled complex WM. (f) Marginal phase-coupled complex WM.

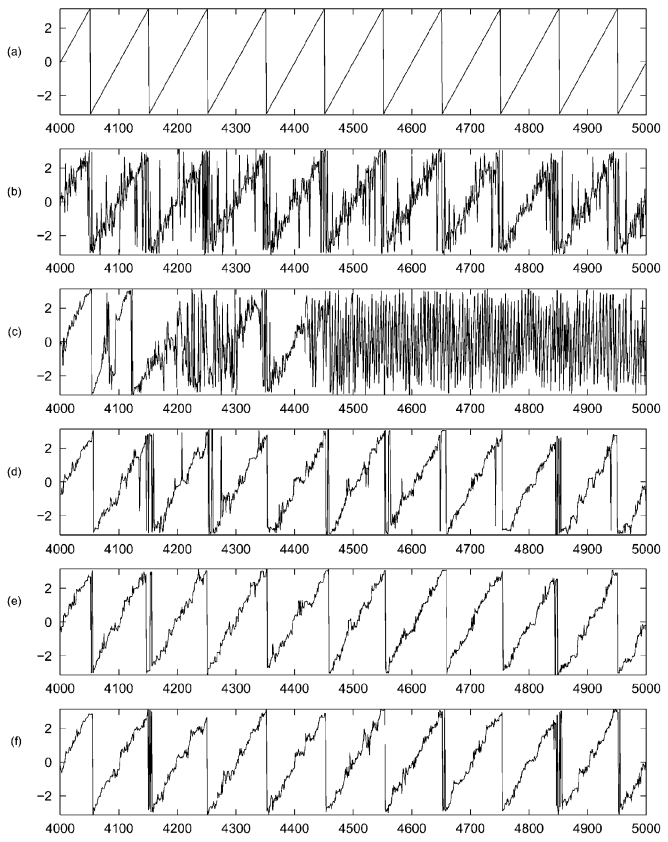

Fig. 7. Phase of the output of the filters for $\alpha = 1.7, \gamma = 0.2$, and $\mu = 0.005$. (a) Original signal. (b) Noisy signal. (c) Linear filter. (d) Marginal complex WM. (e) Real-imaginary coupled complex WM. (f) Marginal phase-coupled complex WM.

these four schemes to compare the results obtained with each one of them. To analyze the convergence properties of the algorithms, we plot the learning curves calculated as the average MSE of 1000 realizations of the experiment. Fig. 4 shows the results for two values of α [(a) $\alpha = 1.5$, (b) $\alpha = 2.0$]. The NLMS algorithm for the linear filter does not appear in the figure since it diverges. On the other hand, the robustness of the marginal phase-coupled complex WM and the real-imaginary coupled complex WM is clearly seen. For the values of α shown, the plot of the MSE keeps almost unaltered, that is, the impulsiveness of the noise does not have a major effect in the performance of the algorithms for $\alpha < 2$. Table I summarizes the average of 2000 values of the MSE after the convergence of the LMS algorithm for the complex filters. These results show the reliability of the complex WM filters in α-stable environments. For this particular application and noise conditions, the marginal phase-coupled and the real-imaginary coupled outperform the marginal complex WM filter.

In Fig. 4, all the LMS updates used a step size of $\mu = 0.005$. The step size has a small effect on the floor error of the complex WM filters, as it is illustrated in Fig. 5, where the learning curves of the LMS algorithm for $\mu = 0.01$ and $\mu = 0.001$ are shown. The plot shows how a higher value of the step size improves the convergence rate of the algorithm without harming the robustness of the filter or modifying significantly the value of the floor error. On the other hand, the LMS algorithm for linear filters has a tradeoff between the convergence rate and the error floor that is dependent on the value of μ.

For illustrative purposes, the real part and the phase of the filter outputs are shown in Figs. 6 and 7, respectively. The plots show 2000 samples of the filter output taken after the LMS algorithm has converged. As it can be seen, the linear filter is not successful at filtering the impulsive noise, whereas the complex WM filters are able to recover the original shape of the signal. The output of the marginal phase-coupled complex WM is the one that resembles the best the original signal.

In the second experiment, adaptive modeling [9] is used to tune the frequency response of the proposed complex WM filters. In order to do this, the system shown in Fig. 8 is used. The Gaussian noise generator provides a complex Gaussian sequence that is fed to both a complex linear filter with the desired frequency response and to the complex WM filter being tuned. The difference between the outputs of the two filters will be the error signal used in an LMS algorithm that will calculate the optimum weights of the complex WM filter. After convergence, the complex WM filter should be a close approximation of the original linear filter in the mean square error sense. Fig. 9 shows the ensemble average learning curves for 1000 realizations of the experiment. The learning curve of a linear filter tuned in the same way has also been included. For this experiment, the complex linear filter $h = [-0.0123 - 0.0123i, -0.0420 - 0.1293i, -0.0108 + 0.0687i, -0.0541 + 0.0744i, 0.2693 - 0.1372i, 0.5998, 0.2693 + 0.1372i, -0.0541 - 0.0744i,$

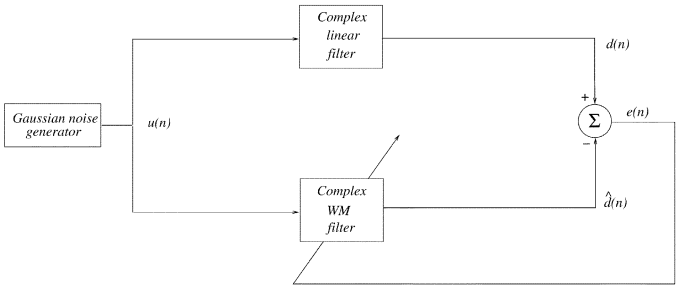

Fig. 8. Block diagram of the adaptive modeling experiment.

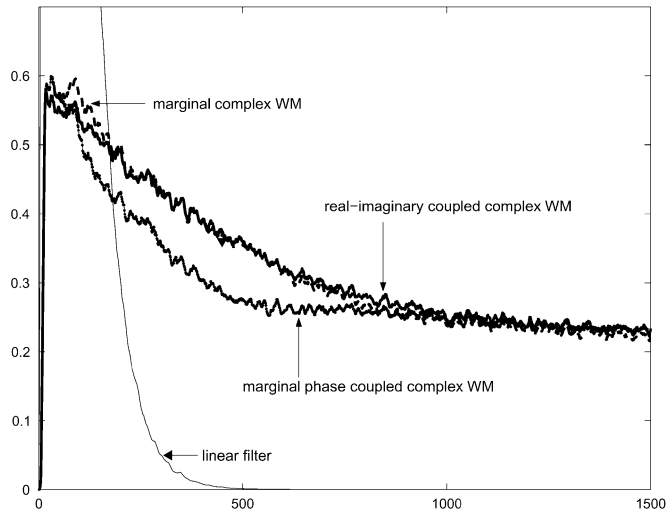

Fig. 9. Learning curves of the LMS algorithm of the marginal phase-coupled complex WM, the real-imaginary coupled complex WM, the marginal complex WM, and a linear filter with $\mu = 0.01$ for the adaptive modeling problem.

$-0.0108 - 0.0687i, -0.0420 + 0.1293i, -0.0123 + 0.0123i]$ was used. This a complex lowpass filter with normalized cut-off frequencies $\omega_1 = -0.4$ and $\omega_2 = 0.7$. The designed complex WM filters have the same number of taps (11). As it was expected, the MSE for the linear filter reaches a minimum of zero. In addition, the floor error for all the complex WM filters is similar.

The frequency response of the complex WM filters, as well as the one of the original linear filter, were calculated as follows: We fed 10 000 samples of complex Gaussian noise to the previously obtained tuned filters, and the spectra of the outputs were calculated using the Welch method [11]. The experiment was repeated 50 times to get an ensemble average, and the results are shown in Fig. 10. The filters have approximately the same bandpass gain, and even though the rejection in the stopband is not as good as the one obtained with the linear filter, the levels reached for the complex WM filters are acceptable.

The real strength of the median filters comes out when the classical model is abandoned and heavy tailed random processes are included. In order to show the power of the filters designed with the LMS algorithm in this adaptive modeling example, the sum of two complex exponentials of magnitude one and two different normalized frequencies (one in the passband (0.2) and one in the stopband (-0.74) of the filters is contaminated with α-stable noise with α taking the values 1, 1.3, 1.7, 2, and $\gamma = 0.1$. If a linear filter were used to filter the clean signal, the output will be a complex exponential of normalized frequency 0.2. This signal is used as a reference to calculate the MSE of the outputs of the complex WM filters and a linear filter in the presence of the noise. Table II shows the average of 100 realizations of the filtering of 200 samples of the noisy signal for each case.

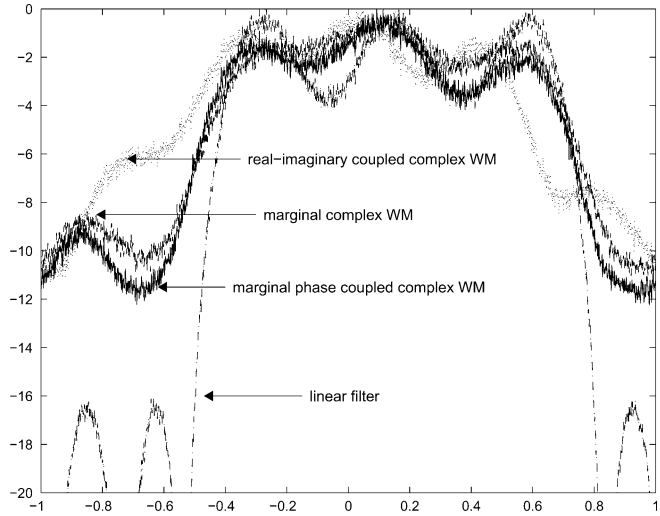

Fig. 10. Frequency response of the complex WM filters for the adaptive modeling problem.

TABLE II
AVERAGE MSE OF THE OUTPUT OF THE COMPLEX WM FILTERS AND THE LINEAR FILTER IN PRESENCE OF α-STABLE NOISE

Filter	$\alpha = 1$	$\alpha = 1.3$	$\alpha = 1.7$	$\alpha = 2$
Linear filter	833.2	6.524	0.623	0.2398
Marginal complex WM	0.8600	0.8079	0.7856	0.7757
Marginal phase coupled complex WM	0.8637	0.8071	0.7727	0.7578
Real-imaginary coupled complex WM	0.5261	0.5192	0.5090	0.5010

As it can be seen, for this application, the real-imaginary coupled complex WM obtains the best results in the presence of α-stable noise with $\alpha < 2$. On the other hand, the linear filter is unable to get rid of the impulsive noise as it is shown in the high values of the MSE of its output. In the Gaussian case, the linear filter shows its superiority.

An example of the real part of the original signal, the noisy signal, and the output of the filters is shown in Fig. 11. The plots show the presence of only one sinusoidal in the outputs and still show some artifacts due to the remaining noise after filtering. The other exponential has been eliminated from the signal, showing the frequency selection capabilities of the complex WM filters.

V. CONCLUSION

This paper introduced novel WM structures admitting complex-valued weights. Two efficient and well-defined robust filtering structures and their LMS optimization were presented. Their performance was demonstrated through examples commonly encountered in signal processing and communication applications.

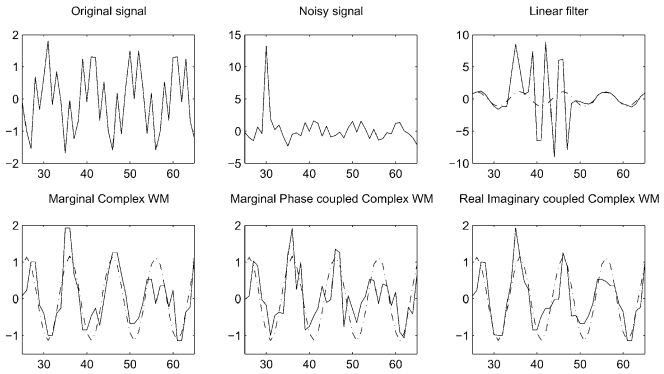

Fig. 11. Real part of the output of the complex WM filters for the adaptive modeling problem with additive α-stable noise ($\alpha = 1$). (The real part of the ideal output is shown in dash-dot.)

The phase-coupled complex WM uses phase coupling between weights and input samples. To calculate the output of this complex filter, a 2-D search in the complex plane is needed, which results in a highly expensive implementation. To overcome this problem, the marginal phase-coupled complex WM filter that separates the optimization problem found in the phase-coupled complex WM into real and imaginary parts, was proposed.

A second definition of complex-valued weighting in WM filters was also presented. It uses the natural coupling characteristic found in complex-valued linear filters to define the real and imaginary parts of the complex WM filter output. This definition has been called real-imaginary coupled complex WM and represents a convenient complex-valued robust filter that exploits the correlation between real and imaginary domains.

The use of either the marginal phase-coupled WM filter or the real-imaginary coupled complex WM filter depends on the specific application as one of the filters might have better performance or may be more convenient than the other in terms of implementation complexity. For instance, if, in a given VLSI system that handles complex-valued data, the circuitry has been set up to work with the magnitude and phase of the complex numbers, the marginal phase-coupled complex WM filter would be the filter to use. On the other hand, if the complex numbers are represented as real and imaginary parts, the real-imaginary coupled complex WM filter would be more suitable for implementation.

In general, the phase coupling and the real-imaginary coupling ideas not only can be used in complex-valued filtering framework based on median filters but in any other complex-valued structure based on other types of nonlinear filters. For instance, it is possible to develop a complex-valued nonlinear filter theory based on *Myriad* [12] using the two coupling techniques proposed in this paper. However, since the median filter is the best understood robust filter, the proposed complex-valued WM filters represent an efficient tool to combat complex-valued non-Gaussian noise.

REFERENCES

[1] V. Barnett, "The ordering of multivariate data," *J. R. Statist. Soc. Assoc.*, vol. 139, pp. 331–354, Feb. 1976.

[2] J. Galambos, "Order statistics of samples from multivariate distributions," *J. Amer. Statist. Assoc.*, vol. 70, pp. 674–680, 1975.

[3] R. C. Hardie and G. R. Arce, "Ranking in $\mathcal{R}^p$ and its use in multivariate image estimation," *IEEE Trans. Circuits Syst. Video Technol.*, vol. 1, pp. 197–208, Feb. 1991.

[4] G. R. Arce, "A general weighted median filter structure admitting real-valued weights," *IEEE Trans. Signal Processing*, vol. 46, pp. 3195–3205, Dec. 1998.

[5] R. Arens, "Complex processes for envelopes of normal noise," in *IRE Trans. Inform. Theory*, vol. IT-3, Sept. 1957, pp. 204–207.

[6] J. Astola, "Matched median filtering," *IEEE Trans. Commun.*, vol. 40, pp. 722–729, Apr. 1992.

[7] H. A. David, *Order Statistics*. New York: Wiley, 1981.

[8] J. Fitch, E. Coyle, and N. Gallagher, "Median filtering by threshold decomposition," *IEEE Trans. Acoust., Speech, Signal Processing*, vol. ASSP-32, pp. 1183–1188, Dec. 1984.

[9] S. Haykin, *Adaptive Filter Theory*. Englewood Cliffs, NJ: Prentice-Hall, 2001.

[10] G. Samorodnitsky and M. S. Taqqu, *Stable Non-Gaussian Random Processes*. London, U.K.: Chapman & Hall, 1994.

[11] P. D. Welch, "The use of fast Fourier transform for the estimation of power spectrum: A method based on time averaging over short modified periodograms," *IEEE Trans. Audio Electroacoust.*, vol. AU-15, pp. 70–73, June 1967.

[12] J. G. Gonzalez and G. R. Arce, "Optimality of the myriad filter in practical impulsive-noise enviroments," *IEEE Trans. Signal Processing*, vol. 49, pp. 438–441, Feb. 2001.

[13] L. Yin and Y. Neuvo, "Fast adaptation and performance characteristics of FIR-WOS hybrid filters," *IEEE Trans. Signal Processing*, vol. 42, pp. 1610–1628, July 1994.

[14] Q. Liu, J. Astola, and Y. Neuvo, "Matched median filter for detecting QAM signals," *IEEE Trans. Commun.*, vol. 43, pp. 7–10, Jan. 1995.

[15] J. Astola, P. Haavisto, and Y. Neuvo, "Vector median filters for complex signal," in *Proc. Int. Conf. Acoust., Speech, Signal Process.*, vol. 2, 1989, pp. 813–816.

[16] B. Smolka, M. Szczepanski, K. N. Plataniotis, and A. N. Venetsanopoulos, "On the fast modified vector median filter," in *Proc. Can. Conf. Electr. Comput. Eng.*, vol. 2, 2001, pp. 1315–1320.

[17] M. Barni, V. Cappellini, and A. Mecocci, "Fast vector median filter based on Euclidean norm approximation," *IEEE Signal Processing Lett.*, vol. 1, pp. 92–94, June 1994.

[18] V. Koivunen, "Nonlinear filtering of multivariate images under robust error criterion," *IEEE Trans. Image Processing*, vol. 5, pp. 1054–1060, June 1996.

[19] S. Agaian, J. Astola, and K. Egiazarian, *Binary Polynomial Transforms and Nonlinear Digital Filters*. New York, NY: Marcel Dekker, 1995.

Sebastian Hoyos (S'02) was born in Cali, Colombia, in 1975. He received the B.S. degree from the Pontificia Universidad Javeriana (PUJ), Bogota, Colombia, in 2000 and the M.S. and Ph.D. degrees from the University of Delaware, Newark, all in electrical engineering, in 2002 and 2004, respectively.

He worked for Lucent Technologies, Inc. from 1999 to 2000 as Technical Manager and Sales Engineer for the Andean region in South America. Simultaneously, he was an Adjunct Professor at the PUJ University, where he lectured on microelectronics and control theory. In the Fall of 2000, he enrolled in the Department of Electrical and Computer Engineering, University of Delaware. During his master and Ph.D. studies, he worked under the PMC-Sierra Inc., the Delaware Research Partnership Program, and the Army Research Laboratory (ARL) Collaborative Technology Alliance (CTA) in Communications and Networks. At the end of the summer of 2004, he joined the Department of Electrical Engineering and Computer Sciences, University of California at Berkeley, where he is a postdoctoral researcher at the Berkeley Wireless Research Center. He has carried out industrial consulting with Conexant Systems Inc., Newport Beach, CA, for the development of the next generation of ultra-wideband communications systems. His research interests include communication systems, wireless communications, sensor network processing, robust signal processing, and mixed-signal high-speed processing and circuit design. For a complete list of his publications and patents, see www.sebastianhoyos.com.

Yinbo Li (S'99) was born in Mudanjiang, China, in 1973. He received the B.S. and M.S. degrees in underwater acoustic and electrical engineering, both with the highest honors, from the Harbin Engineering University, Harbin, China, in 1994 and 1997, respectively.

From 1997 to 1998, he was with the Institute of Acoustics, Chinese Academy of Sciences, Beijing, China, mainly focusing on signal processing and automatic system control. He was a Research and Development engineer with the Beijing Division of Shenzhen Huawei Technology Co., and a key member of the high-end router developing group from 1998 to 1999. He is currently a Research Assistant with the Department of Electrical and Computer Engineering, University of Delaware, Newark. He has been working with industry in the areas of signal processing and optical communications. His research interests include statistical signal processing, nonlinear signal processing and its applications, image processing, and optical and wireless communications.

Jan Bacca (S'03) was born in Pasto, Colombia, in 1977. He received the B.S. degree in electronic engineering from Pontificia Universidad Javeriana, Bogotá, Colombia, in 2001 and the M.E.E. degree from the Department of Electrical and Computer Engineering, University of Delaware, Newark, in 2003, where he is currently pursuing the Ph.D. degree.

Gonzalo R. Arce (F'02) received the Ph.D. degree from Purdue University, West Lafayette, IN, in 1982.

Since 1982, he has been with the faculty of the Department of Electrical and Computer Engineering, University of Delaware, Newark, where he is the Charles Black Evans Professor and Chairman of Electrical and Computer Engineering. His research interests include statistical and nonlinear signal processing, multimedia security, electronic imaging and display, and signal processing for communications.

Dr. Arce received the Whittaker RESNA and the Advanced Telecommunications and Information Distribution (ATIRP) Consortium best paper awards. He received the NSF Research Initiation Award. He was the co-chair of the 2001 EUSIPCO/IEEE Workshop on Nonlinear Signal and Image Processing (NSIP'01), the 1991 SPIE Symposium on Nonlinear Electronic Imaging, and the 2002 and 2003 SPIE ITCOM Conference. He has served as Associate Editor for the IEEE TRANSACTIONS FOR SIGNAL PROCESSING, Senior Editor of the *Applied Signal Processing Journal*, Guest Editor for the IEEE TRANSACTIONS ON IMAGE PROCESSING, and Guest Editor for *Optics Express*.